

# Simulation and experimental validation of droplet dynamics in microchannels of PEM fuel cells

Moosa Ashrafi<sup>1</sup> · Mehrzad Shams<sup>1</sup> · Ali Bozorgnezhad<sup>1</sup> · Goodarz Ahmadi<sup>2</sup>

Received: 9 September 2015 / Accepted: 5 February 2016 / Published online: 18 February 2016  
© Springer-Verlag Berlin Heidelberg 2016

**Abstract** In this study, dynamics of droplets in the channels of proton exchange membrane fuel cells with straight and serpentine flow-fields was investigated. Tapered and filleted channels were suggested for the straight and serpentine flow-fields respectively in order to improve water removal in channels. Surface tension and wall adhesion forces were applied by using the volume of fluid method. The hydrophilic walls and hydrophobic gas diffusion layer were considered. The mechanism of droplets movement with different diameters was studied by using the Weber and capillary numbers in simple and tapered straight channels. It was illustrated that the flooding was reduced in tapered channel due to increase of water removal rate, and available reaction sites improved subsequently. In addition, film flow was formed in the tapered channel more than the simple channel, so pressure fluctuation was decreased in the tapered channel. Moreover, the water coverage ratio of hydrophilic tapered surface was more than the simple channel, which enhanced water removal from the channel. The filleted serpentine channel was introduced to improve water removal from the simple serpentine channel. It was shown by observation of the unsteady and time-averaged two-phase pressure drop that in the filleted serpentine channels, the two-phase pressure drop was far less than the simple serpentine channel, and also the accumulation of water droplets in the elbows was less leading to lower pressure

fluctuation. The numerical simulation results were validated by experiments.

## List of symbols

$A_a$	The area of adhered water to the upper surface of channel
$A_i$	The initial area of the droplet
$Bo$	Bond number
$Ca$	Capillary number
$D$	Diameter (m)
$F$	Source term (N)
$h$	Channel inlet height
$n$	Normal unit vector
$P$	Pressure (Pa)
$R_a$	Adhered water ratio (water coverage ratio)
$S$	Ratio of inlet to outlet height of channel
$t$	Tangential unit vector
$v$	Velocity (m/s)
$We$	Weber number

## Greek letters

$\alpha$	Volume fraction
$\theta$	Contact angle (°)
$\kappa$	Surface curvature
$\mu$	Viscosity (kg/m/s)
$\rho$	Density (kg/m <sup>3</sup> )
$\sigma$	Surface tension (N/m)

## Subscripts

$ch$	Channel
$d$	Droplet
$g$	Gas (air)
$l$	Liquid
$Vol$	Volumetric
$W$	Channel wall

✉ Mehrzad Shams  
shams@kntu.ac.ir

<sup>1</sup> Multiphase Flow Lab, Faculty of Mechanical Engineering, K.N. Toosi University of Technology, No. 17, Pardis St., Mollasadra Ave., Vanak Sq., Tehran 19395-1999, Iran

<sup>2</sup> Department of Mechanical and Aeronautical Engineering, Clarkson University, Potsdam, NY, USA

## 1 Introduction

Proton exchange membrane fuel cell (PEMFC) is a device for converting chemical energy into electrical power. It produces just water and heat as byproducts during its operation. Low operating temperature, high efficiency, and comfortable setup make it popular among all types of fuel cells [1]. However, there are some problems for commercialization of PEMFCs. Flooding of channels is one of these problems causing deficient operation of PEMFCs [2–4].

Water droplets accumulate on cathode side of PEMFCs at high current densities and low operating temperature. Temperature gradient, local pressure and electro-osmotic drag, cause the water to pass through polymer membrane and going to cathode side of PEMFC [5]. Then, the water passes through a gas diffusion layer (GDL) and finally enters the cathode channel. The fuel cell will operate with lower efficiency, if the existed water in the channel accumulates on the GDL surface. On the other hand, the polymer membrane needs to be humidified for maintenance of its ionic conductivity. However, if the existed water is more than the necessity, the flooding occurs. Flooded channel also causes excessive pressure drop. Therefore, channels must be designed in a way that neither flooding nor dehydration occurs in PEMFCs.

In the recent years, water management in the PEMFCs was investigated experimentally by many researchers. Owejan et al. [6] fabricated a PEMFC and investigated water distribution on the channels of cell with neutron imaging. Yamauchi et al. [7] used a triple-serpentine PEMFC and make use of direct visualization of anode and cathode channels to calculate water accumulation in the channels of cell by manual calculation. Hussaini and Wang [8] studied the effects of air stoichiometry, current density and relative humidity on flow patterns of cathode side. Ous and Arcoumanis [9] visualized droplets in a transparent PEMFC. They concluded that droplets are formed in the middle of channels and no water accumulation appears at the end of channels. They also classified droplet detachment velocities based on gas velocity. Akhtar et al. [10] studied several cross sections for the flow-fields. Their results showed that triangular channels not only have no positive result on water removal from channels, but also leads to increase of pressure drop. However, rectangular cross sections lead to moderate pressure drop and better water removal.

Visualization of two-phase flow arises many difficulties in the studying of PEMFCs, so numerical simulations and modeling together with experiments are used for predicting behavior of two-phase flow in the PEMFCs [11]. In numerical simulations, changes are easily made and therefore various conditions can be simulated. Among various methods used for numerical simulation of two-phase flow, the volume of fluid (VOF) method is more utilized

for simulation of PEMFCs. In this method, surface tension and wall adhesion forces are applied. These forces influence the formation of two-phase flow in PEMFCs channels. Zhu et al. [12] simulated a two-dimensional channel with a one-dimensional pore for injection of water from surface of GDL. They studied effects of water injection velocities, airflow rates and pores diameters on droplet movement in the channel. They also studied the effect of these parameters in a three-dimensional channel [13]. Zhou et al. used the VOF method in several studies for analyzing two-phase flow in cathode channels with various designs. They used a three-dimensional model for determining water distribution in serpentine, parallel and interdigitated channels [14–16]. Ding et al. [17] modeled a three-dimensional channel with multi-pores. They concluded that humidity of GDL and shape of the pores affect flow pattern within the channel of PEMFC.

Several models have been introduced to study the droplet dynamics in channels of PEM fuel cells. Theodorakakos et al. [18] analyzed droplet dynamics on the GDL surface both numerically and experimentally. They stated that the GDL surface cannot taken to be smooth due to its relatively low roughness. Kumbur et al. [19] studied droplet dynamics using an analytical model based on balancing of forces. Their results suggested that droplets with relatively more height are removed better than the other droplets, which are relatively filmed. Cho et al. [20] introduced an analytical model of detachment velocity and the forces imposed on droplets comparing the results with experimental data.

In the literature, the movement mechanisms of small and large droplets in micro fuel cells have not been considered and only droplet dynamics in different operating conditions and physical properties were investigated. In the current study, we aim to select the optimum configuration between simple and tapered channels by utilizing movement mechanism of droplets with different diameters in different operating conditions and detecting the dominant force exerted on droplets using the Weber and capillary numbers. To this end, various parameters of both channels are investigated including water adhered to hydrophilic surface, unsteady and time-averaged two-phase pressure drop, departure time of droplet related to its average velocity, which shows water removal rate of channel. Simple serpentine channels with sharp elbows are optimized from the perspective of water management and lowering pressure drop introducing an optimized filleted channel.

## 2 Numerical model

Generally, a PEMFC can be modeled two-dimensionally by means of two methods as illustrated in Fig. 1. The first method is modeling PEMFC in the normal direction of gas

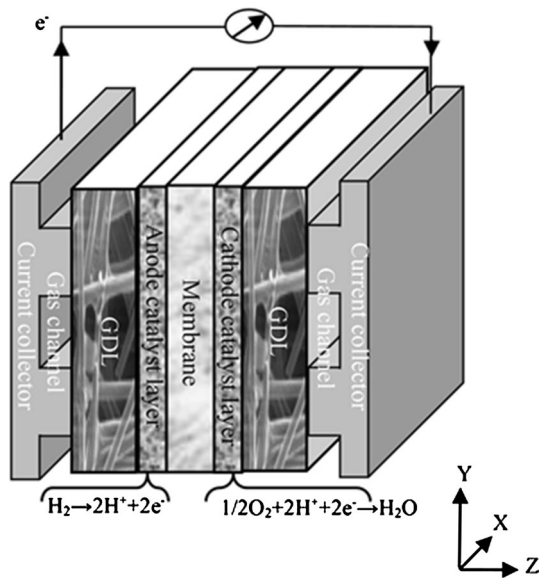


**Fig. 1** Schematic of PEMFC

flow. In this method, the coordinate axes are located in the direction of Y–Z plane. Modeling in the Y–Z plane is used for investigation of species concentration and flow condition in the GDL, catalyst layer and polymer membrane. The second method is two dimensionally modeling of PEMFC in the direction of the gas flow, which is investigated in the plane of X–Z or X–Y. In the present simulations, the gas–liquid two-phase flow is investigated for the cathode channel; therefore, dynamics of droplet is simulated on the surface of GDL in the X–Z plane. Furthermore, the droplet movement on walls and corner of channels is simulated in the X–Y plane.

In current study, tapered parallel channels are introduced in order to improve water removal in simple parallel flow-fields. As the conditions in parallel channels are similar to single channels, a single channel is analyzed and compared. Accordingly, dynamics of droplet movement

**Table 1** Dimensions of simulated straight channels

Parameter	Tapered channel	Simple channel
Inlet height (μm)	250	250
Outlet height (μm)	125	250
Channel length (μm)	1000	1000

in the single channel of straight flow-field and the droplet dispersion on the elbows of serpentine flow-field were simulated in the X–Z and X–Y plane, respectively. The tapered and filleted channels were introduced for the PEMFCs with the straight-parallel and serpentine flow-fields respectively, for improvement of water removal from the GDL surface. The schematic of simple and tapered straight channels is shown in Fig. 2 and their dimensions are listed in Table 1.

In the serpentine flow-fields, water droplets accumulates on the channels corners [21] and occupy the permeation surface of GDL. Therefore, less air reaches to the catalyst layer, and the power of fuel cell decreases subsequently. Filletting the channel corners is suggested for reducing this excessive accumulation of water. Five passes are considered for simulation of two-phase flow in the serpentine channels for the simple and filleted channels as shown in Fig. 3. The inner and outer radii of channel corners are 0.5 and 2 mm, respectively.

**2.1 Physical assumptions**

The interaction of wall adhesion and surface tension leads to different contact angles between solid and liquid phases at interface of gas–liquid–solid phases. If surface tension is greater than wall adhesion, contact angle will be >90° and the surface is defined as a hydrophobic surface. Otherwise, contact angle will be <90° and the surface is defined as a hydrophilic surface. The schematic of hydrophobic and hydrophilic surfaces is shown in Fig. 4.

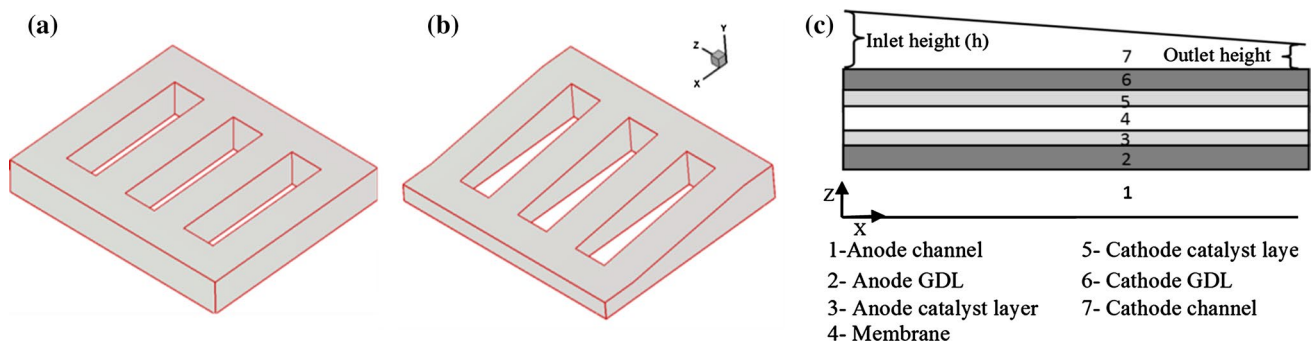


**Fig. 2** a Schematic of a straight simple, b tapered and c simulated cathode channels of PEMFC

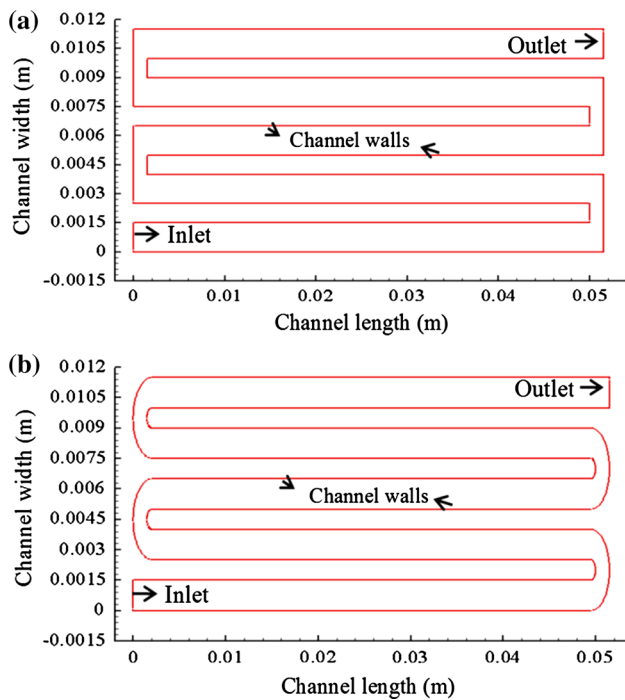


**Fig. 3** Schematic of **a** simple and **b** filleted channel of serpentine flow-field

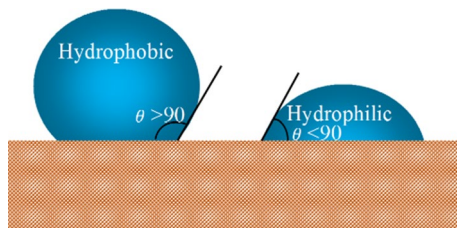


**Fig. 4** Hydrophilic and hydrophobic surfaces

On the hydrophobic surfaces, droplets reach a critical diameter, and then they are removed. This critical diameter depends on mass flow rates of water and air [22]. Otherwise if the surface is hydrophilic, droplets do not detach from the surface easily. For this reason, if the GDL surface is hydrophilic, the amount of oxygen transferred to the catalyst layer, and subsequently the reaction rate will be decreased. According to this behavior of water droplet, the GDL surface should be hydrophobic. The hydrophobicity of GDL is different for various materials, which is typically between  $120^\circ$  and  $145^\circ$ . The contact angle between droplets and channel walls is an important parameter for water management in channels. Water film formation along the channel is dictated theoretically by the Concus–Finn condition [23]:

$$\theta + \varphi_{\text{half}} < 90 \quad (1)$$

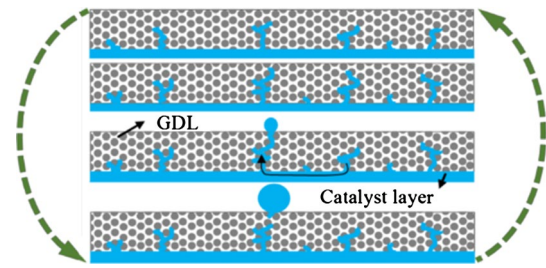


**Fig. 5** Mechanism of droplet formation on the GDL surface

where  $\theta$  is contact angle between the water droplet and the channel walls and  $\varphi_{\text{half}}$  is half-angle formed by the channel corner. For a rectangular channel  $\varphi_{\text{half}}$  is equal to  $45^\circ$ . Therefore,  $\theta$  has to be lower than  $45^\circ$  in order to start film formation along the flow channels. In PEMFCs, walls are usually hydrophilic and further hydrophilicity of the walls surfaces is desired for proper water management since the film flow on the walls is a preferable flow pattern for water removal [17].

Litster et al. [24] concluded that transmission of water to the channel and its emergence on the GDL surface mainly is done by fingering and channeling mechanisms. The droplets gradually become larger and at a certain diameter, which depends on airflow and water flow rate, begin to move and this process is repeated as shown in Fig. 5.

In the present simulations, standard air enters into the channel and pure water is considered as the byproduct of chemical reaction. According to the channel dimensions and flow rates, the Reynolds number is  $<650$ ; therefore the flow regimes are considered laminar [25]. Gas mixture is considered incompressible since the pressure gradient is very small. Heat transfer and its effect on the phase change from liquid to vapor and conversely are ignored in order to report purely hydrodynamic study of droplet.

## 2.2 The governing equations

Two immiscible fluids can be simulated with solving a set of momentum equations using the volume of fluid (VOF) method. The volume fraction of each phase and the interface between them can be followed in the entire solution domain subsequently. Mass conservation equation is,

$$\frac{\partial \rho}{\partial t} + \nabla \cdot (\rho \vec{v}) = 0 \quad (2)$$

In the gas–liquid flows, mixture density is defined as:

$$\rho = \alpha_l \rho_l + \alpha_g \rho_g \quad (3)$$

$\alpha$  is the volume fraction of each phase, which subscripts l and g represent liquid and gas phases, respectively. The volume fraction of each phase is given by:

$$\alpha_l + \alpha_g = 1 \quad (4)$$

Volume fraction continuity equation is,

$$\frac{\partial(\alpha_l \rho_l)}{\partial t} + \nabla \cdot (\alpha_l \rho_l \vec{v}_l) = 0 \quad (5)$$

Then the volume fraction conservation equation for the air phase is derived, if subscript l is replaced by g.

Momentum conservation equation is,

$$\begin{aligned} \frac{\partial(\rho \vec{v})}{\partial t} + \nabla \cdot (\rho \vec{v} \vec{v}) \\ = -\nabla p + \mu \nabla \cdot (\nabla \cdot \vec{v} + \nabla \cdot \vec{v}^T) + \rho \vec{g} + \vec{F} \end{aligned} \quad (6)$$

$P$  is static pressure and  $F$  is source term, which is the surface tension and wall adhesion forces in the present simulations.  $\mu$  is the dynamic viscosity and given by

$$\mu = \alpha_l \mu_l + \alpha_g \mu_g \quad (7)$$

The continuum surface force (CSF) model which is proposed by Brackbill et al. [26] considers the surface tension effect. In this model, surface tension is applied as a source term in the momentum Eq. (6) given by,

$$\vec{F}_{\text{Vol}} = \sigma \left( \frac{\rho_l \kappa_1 \nabla \alpha_l}{1/2(\rho_l + \rho_g)} \right) \quad (8)$$

In the Eq. (8),  $\sigma$  is the surface tension coefficient and  $\kappa_1$  is the surface curvature of liquid droplet defined in terms of the divergence of unit normal  $\vec{n}_l$ , given by,

$$\kappa_1 = \nabla \cdot (\vec{n}_l) \quad (9)$$

The unit normal is given by,

$$\vec{n}_l = \frac{\nabla \alpha_l}{|\nabla \alpha_l|} \quad (10)$$

Wall adhesion effects are considered by adjusting the surface curvature near the wall which this method has been proposed by Youngs [27]. The local curvature of this interface is determined by the static contact angle  $\theta_w$ , which is the angle between the wall and the tangent of the interface at the wall. The surface normal,  $\vec{n}$  for the wall is given by,

$$\vec{n} = \vec{n}_w \cos \theta_w + \vec{t}_w \sin \theta_w \quad (11)$$

where  $\vec{n}_w$  and  $\vec{t}_w$  are the unit vectors normal and tangential to the wall surface, respectively.

In the analysis of forces exerted on the droplet in the channel, two dimensionless numbers are used as follows,

$$Ca = \frac{\mu_l v_l}{\sigma} \quad (12)$$

$$We = \frac{\rho_l v_l^2 D_d}{\sigma} \quad (13)$$

The  $Ca$  is the capillary number which is defined as a ratio of viscous and surface tension forces. The  $We$  is the Weber number which is defined as a ratio of inertia and surface tension forces.

### 2.3 Solution methodology

The finite volume method is utilized to discretize governing equations. The pressure-based segregated algorithm is used to solve the Navier–Stokes and volume fraction equations consecutively. Two-phase flow in the channels is simulated numerically by using VOF method based on explicit-scheme. The PISO algorithm (pressure-implicit with splitting of operators) couples the pressure and velocity. For discretizing pressure, the pressure staggering option (PRESTO!) is selected. To minimize numerical diffusion, the momentum equation is solved by quick differencing scheme. The first-order implicit time marching scheme is used for solving the unsteady formulation. Simulations are performed by FLUENT<sup>®</sup>6.3.26 [28].

### 2.4 Validation of grid and time step independency

In order to verify solution independency from computational grids and time step, three grids and time steps are utilized as shown in Table 2. As shown in Fig. 6, the Richardson extrapolation [29] with Grid Convergence Index (GCI) and Time Convergence Index (TCI) are used to estimate water volume fraction in the outlet for both the grid size and time step of zero. The results of GCI and TCI show that the estimated water volume fraction in the outlet are 0.704695 and 0.7045 with errors of 0.036 and 0.02 % respectively. Therefore, the grid with 10,000 cell is verified for current simulation and further grids will not have substantial effect on the accuracy of results. The results also suggest that the time step of  $10^{-8}$  (s) lead to independency of solution from the time step, and further decrease of time step value is not logical regarding the computational time. For ensuring the solution convergence in each time step, the number of iterations in each time step set as 200. The convergence criteria for all parameters considered  $10^{-6}$ .

**Table 2** Grid numbers and time steps for verification study

Grid numbers	Time steps (s)
Mesh 1: 14,000	Time step 1: $5 \times 10^{-9}$
Mesh 2: 10,000	Time step 2: $1 \times 10^{-8}$
Mesh 3: 7142	Time step 3: $2 \times 10^{-8}$

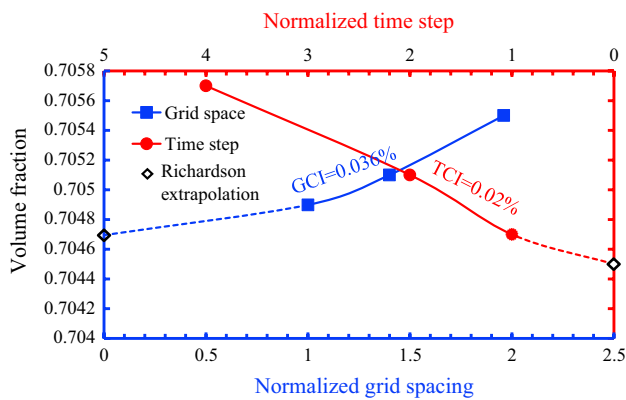


**Fig. 6** Grid and time step independence test for the volume fraction of water in the outlet at  $t = 450 \mu\text{s}$ . A droplet with the radius of 125  $\mu\text{m}$  moves on the GDL at the airflow velocity of 5 m/s

## 2.5 Operational and boundary conditions

In the present simulation, a parabolic profile is set for the boundary condition of the inlet air velocity. The maximum velocity is in the middle of channel and in this study, it was named as the inlet velocity of channel. The atmospheric pressure was applied to the channel outlet as outlet boundary condition and no-slip boundary condition and also wall adhesion are applied to the walls. In Table 3, the values of all parameters and constants used in the simulations are given. The time step of solution was selected  $10^{-8}$  (s) in order that the Courant Number be  $<0.25$ . In the present simulations the initial location of the droplets is set on the channel inlet and the initial velocities of them are zero, and no air flow exists in the channel while the air flow enters the channel in  $t = 0$ .

**Table 3** Values of all parameters in the simulations

Parameter	Value	Unit
Air density	1.225	$\text{kg}/\text{m}^3$
Air viscosity	$1.78 \times 10^{-5}$	$\text{kg}/(\text{m s})$
Droplet radii	31.25, 50, 125	$\mu\text{m}$
Gravity	9.81	$\text{m}/\text{s}^2$
Inlet velocities of air	5, 10, 15	$\text{m}/\text{s}$
Operating temperature	298.3	Kelvin
Static contact angle of water and hydrophilic surface	40	Degrees
Static contact angle of water and hydrophobic surface	140	Degrees
Surface tension	0.0719	$\text{N}/\text{m}$
Water density	998.2	$\text{kg}/\text{m}^3$
Water viscosity	0.001003	$\text{kg}/(\text{m s})$

## 3 Results and discussion

In this study, straight and serpentine channels are investigated, and optimized channels are introduced for both of them from a water management and pressure drop perspective.

### 3.1 Straight channel

In this section, a simple straight channel is studied first and in the next part, a tapered channel is introduced as an alternative and optimized channel for improved water management in straight channels.

#### 3.1.1 Simple channel

The movement of a droplet with an initial radius of  $h/2$  in the simple rectangular channel is shown in Fig. 7.

For the velocity of 5 m/s, it is observed that three mechanisms are occurring simultaneously. First, the receding point is moving in the flow direction. Second, the upper part of the droplet has an ascending motion and along with the entire droplet moves forward. Third, the advancing point has a forward motion. The reason of these mechanisms can be identified using the streamlines and the contour of relative pressure shown Fig. 8. The pressure at the contact area of air and the backside of droplet is high while at the front of the droplet is low leading to a forward driving force. According to Fig. 9a, which represents capillary and Weber numbers respectively, the surface tension force other than the contact area of air and droplet is dominant forces throughout of the droplet in  $t = 2 \mu\text{s}$  and therefore, the shape of droplet remains unchanged. Simultaneously, the airflow passing through the space above the droplet creates an inclined shear force toward the top, which causes divergence of the streamlines at the top and bottom of the droplet. So the top of droplet moves to upward.

Because of pressure drop, which is caused by inducing vortex of airflow, the receding contact angle of droplet increases. As seen in Fig. 7 for the air velocity of 5 m/s at state (d), streamlines are downward at the top of droplet, so the viscous and inertial forces are downward at this moment. Consequently, the top of droplet moves downward to the lower wall of channel and forms film flow on the GDL surface.

As shown in Fig. 7 for the air velocity of 10 and 15 m/s, initial states of droplets compared to the first case are more unstable due to the amplification of inlet velocity. In addition, the Weber number is increased (Fig. 9b) and that is interpreted as the momentum force increment because of the constant surface tension in this study. In the early

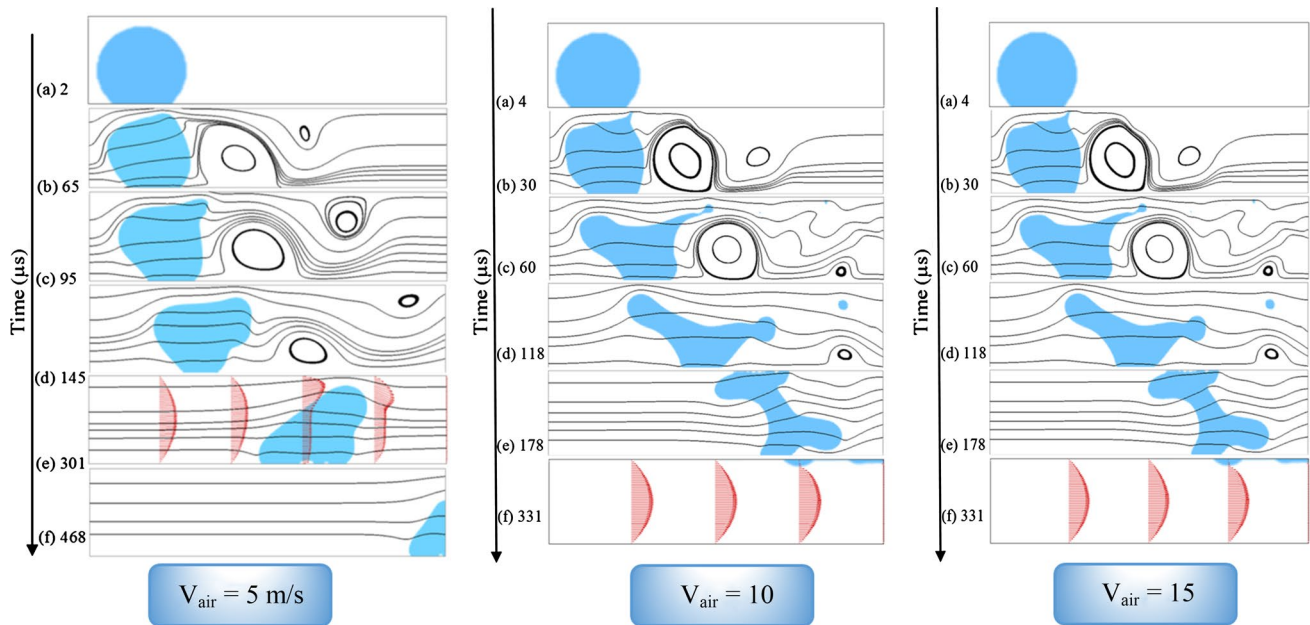


**Fig. 7** Movement of a droplet with the radius of  $h/2$  in the simple channel over time (blue, red and black colors are referred to droplets, velocity profile and streamlines, respectively) (color figure online)

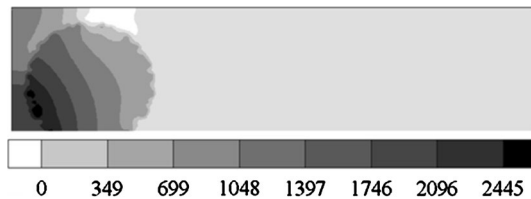


**Fig. 8** Contour of relative pressure in the simple channel for the air velocity of 5 m/s at state (a) (Fig. 7)

moments of droplet movement for the velocities of 10 and 15 m/s, the air passes through the top of droplet and then departs to its front side. The advancing contact angle of droplet is decreased due to the negative component of the airflow velocity that is produced by the large clockwise vortex, which is in the front side of the droplet as shown in Fig. 7. Decrease of advancing contact angle will continue until the impact of impinging momentum on the backside of droplet is greater than its impact on the front side of droplet. Then, the advancing contact angle of droplet is gradually increased, because the effect of large vortex of droplet front side is diminishing as shown in Fig. 7 for states (d), whereas the shear force of the airflow and impinging momentum to the droplet is increasing as shown in Fig. 9b. Deformation of the upper part of droplet occurs faster due to the larger capillary number; in other words, that is because of larger shear force as shown in Fig. 9b. There is an important difference with the previous case; In this case, the separated parts of the primary droplet

increase due to the more shear force exerted on the droplet. The upper surface absorbs impinging droplets, which are produced on the GDL because the upper surface is hydrophilic. Therefore, effective surface for oxygen passage and water removal increases, and film flow is formed on the upper surface of channel as shown in Fig. 7.

It should be noted that the ratio of gravitational force to surface tension force ( $Bo = \rho_l g D_d^2 / \sigma$ ), in the biggest droplet in the channel, with the radius of  $h/2$ , is  $8.52 \times 10^{-3}$ , which is the maximum value compared to the other droplets. However, this small value verifies that the surface tension force is more effective than gravitational force on the dynamics of droplet movement in all states.

The movement of a droplet with an initial radius of  $h/5$  in the simple rectangular channel with the velocities of 5 and 15 m/s over time is shown in Fig. 10. The difference between the movement mechanisms of droplets with different radii is characterized by comparing the movement of droplets with the radii of  $h/2$  and  $h/5$  over time. In Fig. 7, the formation of vortex inside the droplet is not observed, because the momentum force of air overcomes on the shear force. The main mechanism of droplet movement is translational since the bulk of droplet is exposed to the momentum force. However, as the droplet is getting smaller, the shear force is being applied to the droplet surface, so this force creates a rolling moving within the droplet as shown in Fig. 10. In this case, rolling mechanism is the dominant mechanism of movement and together with the translational mechanism cause the droplet to move. Unlike the larger droplets, the film flow is not formed, because the

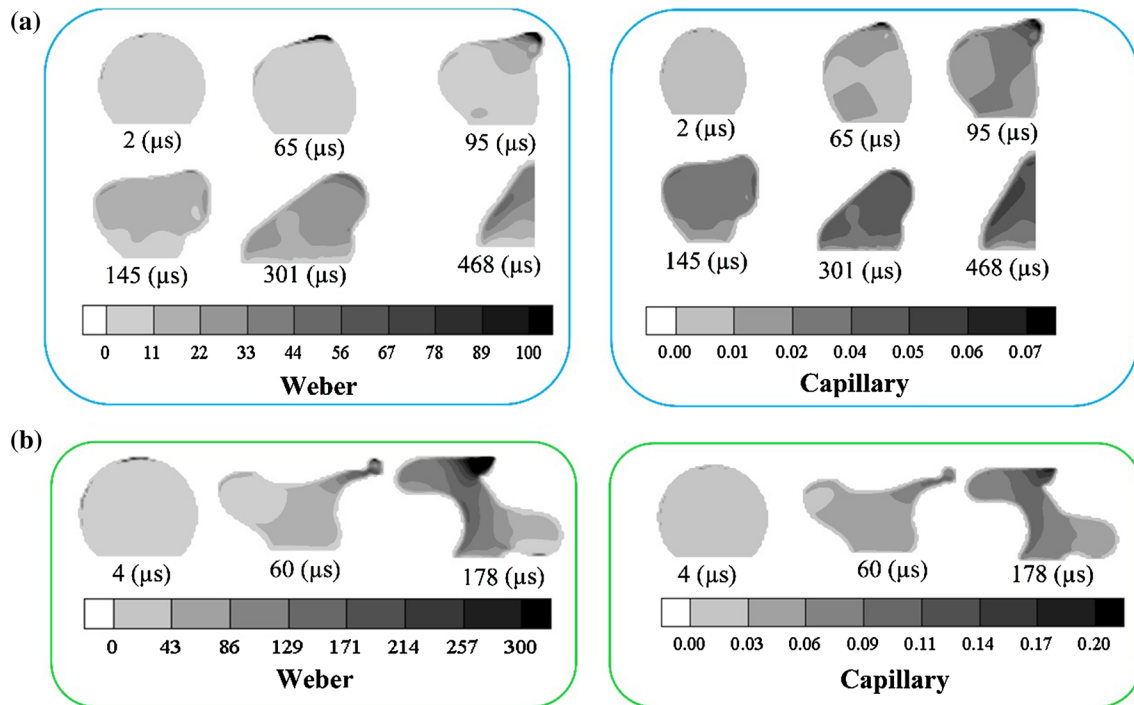
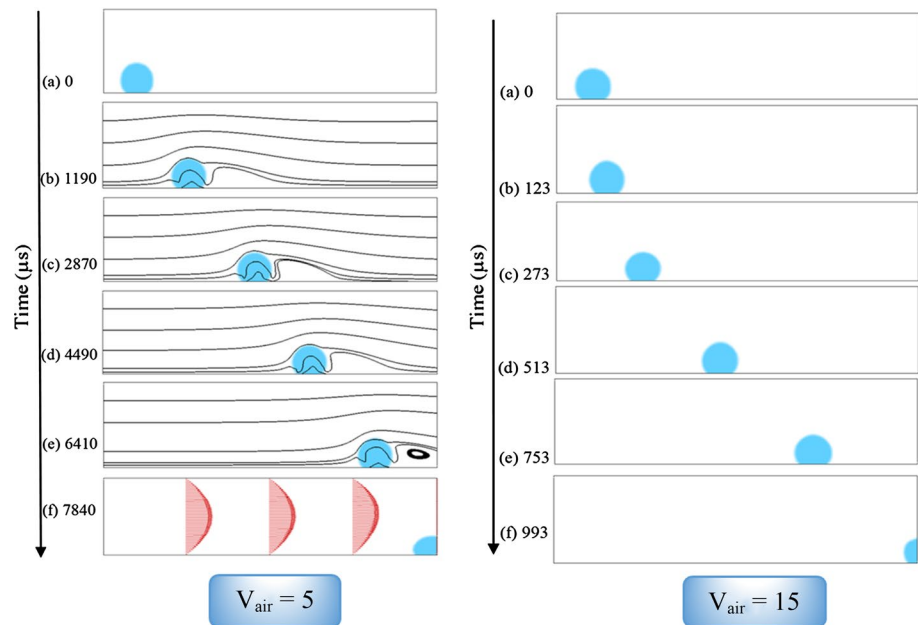


**Fig. 9** Contour of capillary and Weber number; air velocity: **a** 5 m/s, **b** 10 m/s

**Fig. 10** Movement of a droplet with the radius of  $h/5$  in the simple channel over time (*blue, red and black colors* are referred to droplets, velocity profile and streamlines, respectively) (color figure online)



capillary and Weber numbers were reduced compared to the larger droplet as shown in Fig. 11.

The movement of a droplet with an initial radius of  $h/8$  in the simple rectangular channel with the velocity of 15 m/s is shown in Fig. 12. In this case, the movement of droplet is similar to the movement of droplet with the radius

of  $h/5$ . Generally, as the droplet is getting smaller, the surface tension and wall adhesion forces increase compared to the momentum force and hence, the rolling mechanism is appeared which is the dominant mechanism of the droplet movement. The change in the mechanism of droplet movement mainly affects the velocity of droplet in the channel.



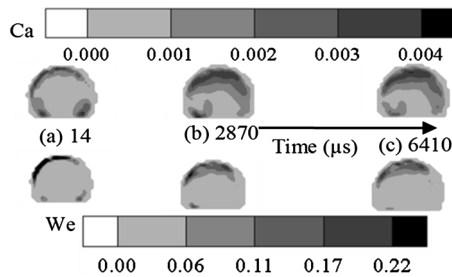


**Fig. 11** Contour of Weber and capillary number of a droplet with the radius of  $h/5$  at the air velocity of 5 m/s

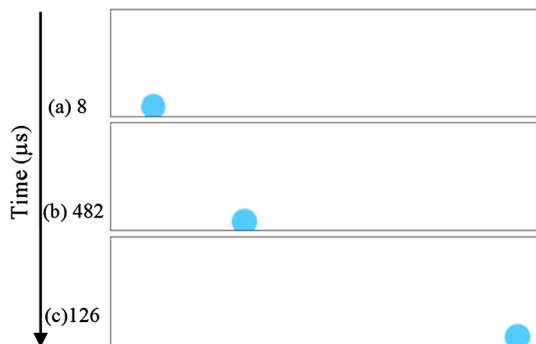


**Fig. 12** Movement of a droplet with the radius of  $h/8$  and velocity of 15 m/s in the simple channel over time (blue color is referred to the droplet) (color figure online)

### 3.1.2 Tapered channel

Transfers of reactant gases to the catalyst layer and water to the channel are through the porous medium. Slow nature of this phenomenon limits the efficiency of PEMFCs. Therefore, some efforts to the transfer of chemical species through porous medium using forced convection are performed. The most important innovation in this area is the interdigitated flow-field, where by blocking the end of channels, reactant gases have to pass through the porous medium to reach to the channel outlet. This forced convection flow improves the transfer of reactant gases to the catalyst layer and water movement toward the channel as well. However, the forced convection flow in porous medium leads to a large pressure drop along the path. Therefore, for compensating this pressure drop, a stronger compressor is required. To mitigate this problem, a proposed solution in the straight flow-fields, which have lower pressure drop compared to serpentine flow-fields, is the utilization of tapered channel. By reducing the cross section area of channel, reactant gases are forced to pass through the porous medium, which has two important effects on the performance of PEMFCs. First, make an easier transfer of reactant gases to the catalyst layer, which results in an improvement in the performance of chemical

reactions in this layer. Second, the forced convection in the porous layer and the resulting shear stress play an important role in the removing of the generated water from the reaction zone and better heat management in this layer. In the following, this novel design in the straight flow-field is investigated and its effects on the dynamics of droplet movement, departure time of droplet, droplet velocity, and two-phase pressure drop are identified.

The schematics of a simple straight flow-field and a tapered channel flow-field are shown in Fig. 2. The ratio of inlet to outlet height of the channel is defined as  $S_{ch}$ . Simulations conducted by Shateri Amiri [30] revealed that for the  $S_{ch}$  of 0.5, pressure drop in the channel is low while the velocity is high. Therefore, in this section, the droplets with diameters and velocities similar to the simple channels are simulated for the  $S_{ch}$  of 0.5.

The movement of a droplet with an initial radius of  $h/2$  in the tapered channel with the velocity of 5 m/s is shown in Fig. 13. It is observed that the mechanism of droplet movement is similar to simple channel. Unlike the simple channel, the film flow is formed on the upper surface of channel. Water adheres to the upper surface because in the tapered channel, the height of channel is lower than the simple channel that causes the viscous and momentum forces to have a significant increase compared to the simple channel, as shown in Fig. 13.

The movements of droplets with the initial radii of  $h/5$  and  $h/8$  in the tapered channel with the velocity of 5 m/s are shown in Fig. 14. The motion mechanism of the small droplets inside the tapered channel is rolling, which is similar to the simple channel, because the surface tension is the dominant force acting on the droplet.

**3.1.2.1 Effect of tapering on departure time of droplet** The times required to complete departure of droplets with different diameters and velocities in the simple and tapered channels are shown in Fig. 15. The time that there is no water on the hydrophobic surface is considered as the departure time. It can be concluded with respect to Fig. 15 that the departure time of all droplets decreases with increase of the inlet flow rate. In other words, the average velocity of the droplets increases with the increase of the inlet flow rate. It is concluded that the departure time in the tapered channel is less than the simple channel for a specified diameter. Therefore, the water removal rate and available reaction sites increase. Due to the change in the mechanism of droplet motion from the translational to the rolling mechanism, departure time for the smaller droplets is much further than the largest.

**3.1.2.2 Effect of tapering on pressure drop and pressure fluctuation** The pressure drop over the departure time for the droplet with the radius of  $h/2$  is shown in Fig. 16a. It is observed that by increasing the air velocity, the pressure drop

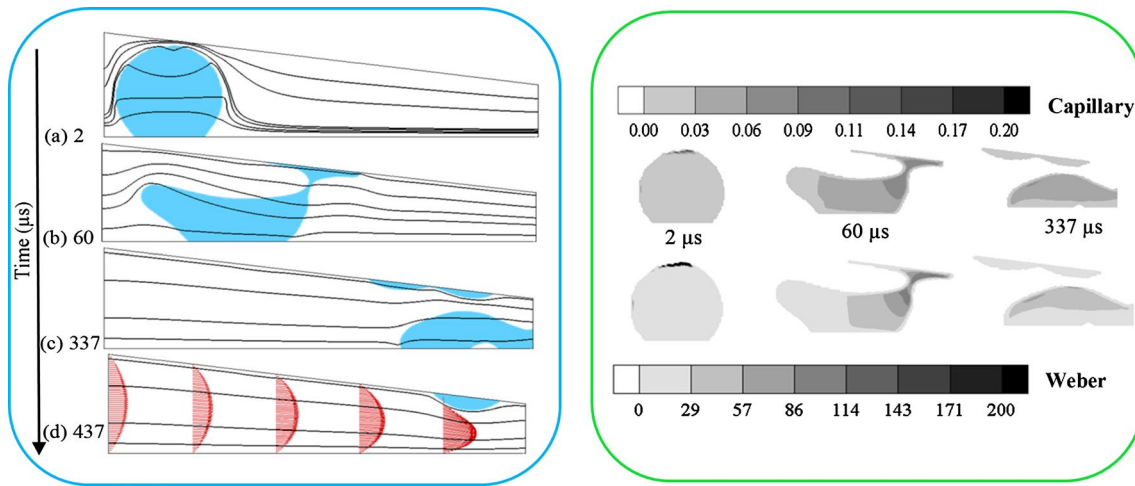


**Fig. 13** Movement of a droplet with the radius of  $h/2$  and velocity of 5 m/s in the tapered channel over time and contour of Weber and capillary of this state (*blue, red and black colors are referred to droplets, velocity profile and streamlines, respectively*) (color figure online)

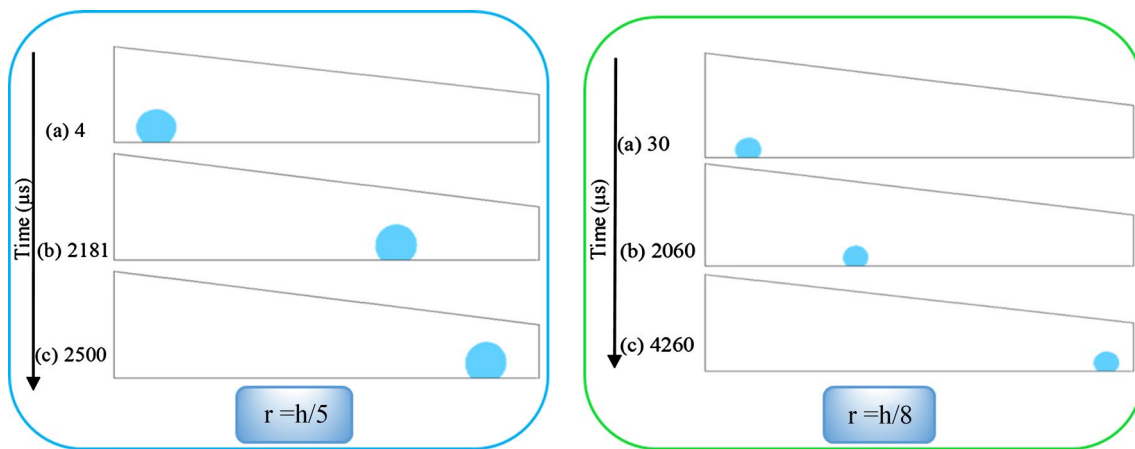


**Fig. 14** Movement of a droplet at the air velocity of 5 m/s in the tapered channel over time (*blue colored is referred to the droplet*) (color figure online)

in both tapered and simple channel is increased significantly. At the beginning of droplet movement in the tapered channel, pressure drop is further than the simple channel. However, the pressure drop and pressure fluctuation are getting lower than the simple channel by dispersing of the droplet over the departure time because of further film flow formation on the upper surface compared to the simple channel, which is desirable for the water removal of PEMFCs. The pressure drop of tapered channel at the end of droplet movement is further than simple channel due to the lower height of channel outlet. The pressure drop over the departure time is shown in Fig. 16b for a droplet with the radius of  $h/5$ . The pressure drop is similar to the previous case. However, the fluctuation of pressure drop over the departure time is lower. Since the upper part of the droplet is more open for the airflow passage. As seen in Figs. 10 and 14, the droplet with the radius of  $h/5$  retains

its shape because of the domination of surface tension force; therefore, the pressure fluctuation decreases. Similarly for this radius, the pressure drop increases at the end of tapered channel, since the height of channel is lower than inlet, and droplet all over the channel keep its shape, therefore less area exists for air passage, and then the pressure drop increases. However, generally the pressure drop of tapered channel is not more than the simple channel substantially.

**3.1.2.3 Effect of tapering on the adhered water to the hydrophilic surface** As the upper surface of channels is hydrophilic, it absorbs impinging droplets forming film flow on this surface, which is desirable for water management of PEMFCs. The adhered water ratio (water coverage ratio) is defined as,

$$R_a = \frac{A_a}{A_i} \times 100 \quad (14)$$

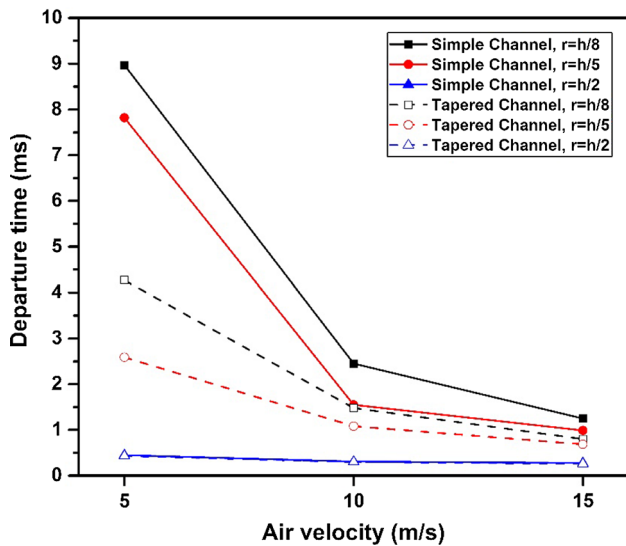


**Fig. 15** Departure time of droplets with different diameters and velocities in the tapered channels

where  $A_a$  is the area of adhered water to the upper surface of channel, and  $A_i$  is the initial area of the droplet. The water removal from the surface of GDL and effective surface for passage of reactant gases from the GDL will decrease, if the adhered water ratio ( $R_a$ ) decreases. Figure 17 shows the amount of adhered water to the upper surface of simple and tapered channels.

The amount of adhered water increases by increasing the airflow velocity since the amount of momentum force of air increases and dominates to surface tension force of droplet; so droplet is easily detached and dispersed on the upper wall. In addition,  $R_a$  increases by tapering of channel because the height of channel decreases in the tapered channels. No water adheres to the upper surface at the

velocity of 5 m/s for simple channel unlike the tapered channel; therefore the amount of water removal and surface available for gas transport decrease for the simple channel.

### 3.2 Serpentine channels

In this section, droplets dispersion in the serpentine channel and influence of changing simple rectangular corners to the rounded corners on the two-phase flow are investigated. Channel dimensions are shown in Fig. 3. Inlet velocity is parabolic and its maximum is 0.5 m/s.

In some areas of flow-field that airflow does not pass through there, the momentum and viscous forces will be less than other areas. Therefore, the probability of water flooding is high in these areas. By use of a steady state and single-phase simulation of airflow, these areas are identified. The velocity contours of simple and filleted serpentine flow-fields are shown in Fig. 18. It is observed that the magnitude of velocity is less than a quarter of inlet velocity at the corners. A strategy to remove these areas, is filleting the elbows of the channels corresponding to the streamlines. In this study, the effect of filleting of channels on single-phase flow pressure drop, unsteady and time-averaged pressure drop of two-phase flow, water coverage ratio of elbows and flow regimes in channels are investigated.

The droplet movement inside the simple channels is shown in Fig. 19. In the experimental studies conducted by Bozorgnezhad et al. [21, 31], it was found that droplets mainly form at the elbows of channel. In the present simulation, droplets are located at the elbows of channel at different moments, which are proportional to water generation rate in the fuel cell. The water generation rate of this simulation is  $2 \times 10^{-6}$  kg/s for the current density of  $0.8 \text{ A/cm}^2$ . Then, droplets move in the channel over time and ultimately adhere to the corner of channel, because airflow is

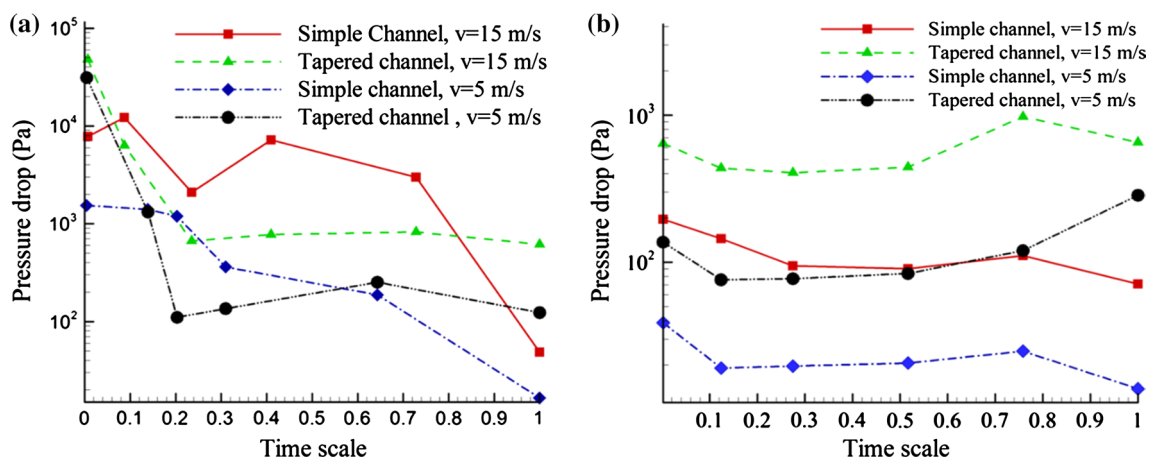


**Fig. 16** Pressure drop over departure time for the droplet with radius of a  $h/2$  and b  $h/5$

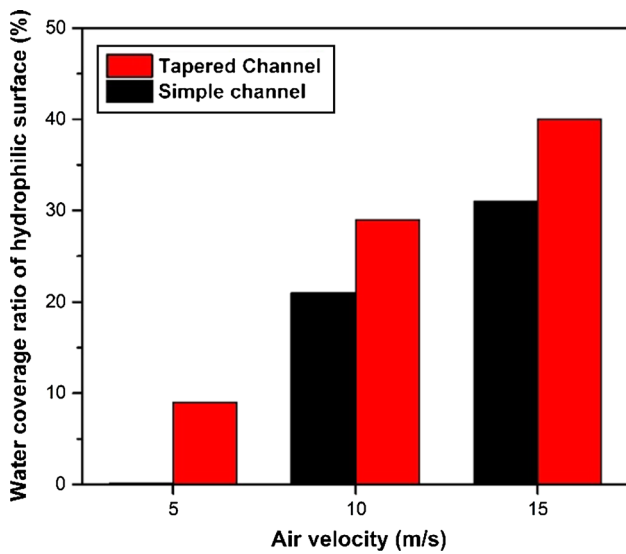


**Fig. 17** Amount of adhered water to hydrophilic surface (water coverage ratio) of tapered and simple channel

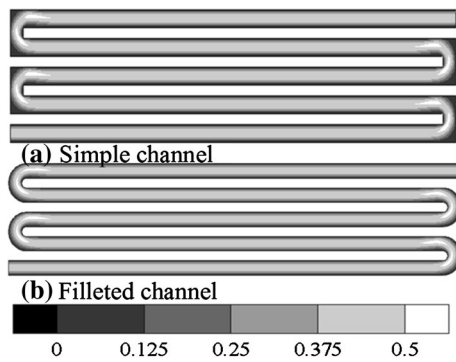


**Fig. 18** Velocity contour of single serpentine channel PEMFC

slow in these parts, which reduces the shear and momentum forces compared with the surface tension force. In other words, at these locations the Weber and capillary numbers are lower than elsewhere. The droplet dispersion within the filleted channels in the same conditions of simple channels is shown in Fig. 20. The airflow passes through the corner of filleted channels more than the simple channel; therefore, shear and momentum forces increase, and droplets do not accumulate in the corners.

### 3.2.1 Effect of filleting elbows on water coverage ratio

The water coverage ratio of elbows can be used for better understanding the effect of filleting channels. The water coverage ratio of elbows is the ratio of the area covered by water in the channel elbows to the area of channel elbows. This value is calculated by using the numerical result. As

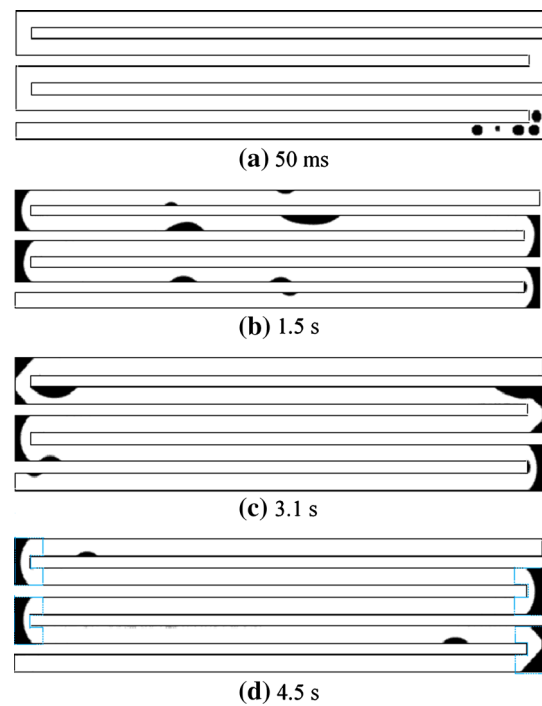


**Fig. 19** Dispersion of droplets in the simple serpentine channel over time

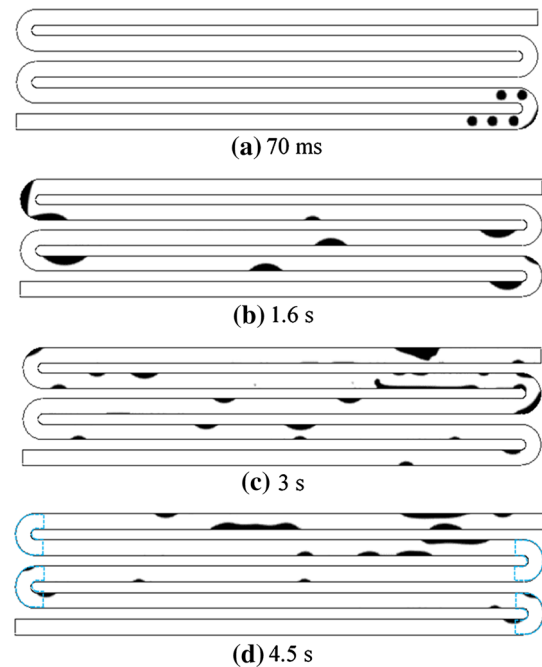


**Fig. 20** Dispersion of droplets in the filleted serpentine channel over time

shown in Fig. 19d, droplets adhere to the channel elbows at the final state. In this state, the water coverage ratio of elbows is 70 %, so only 30 % of the total area of this

location is open for the passage of oxygen. In the final state of the filleted serpentine channel, which corresponds to Fig. 20d, the water coverage ratio of elbows is 12 %. Therefore, there is no water in the 88 % of elbow, and the area of oxygen passage has significantly increased consequently.

### 3.2.2 Effect of filleting of elbows on pressure drop

One of the most important parameters in design of flow-fields is pressure drop in channels. Here, the steady-state single phase pressure drop and also the two-phase pressure drop for simple and filleted serpentine channels are compared. As shown in Fig. 21a, the single phase pressure drop in filleted channel is less than simple channel since the minor loss of pressure drop in elbows is lower. The filleted serpentine channels also have other advantage to simple serpentine channels. As shown in Fig. 21a, in the presence of water in the channel, time-averaged pressure drop of single and filleted serpentine channels increase substantially showing the great effect of two-phase flow on pressure drop. But, it is showed that the two-phase pressure drop of filleted serpentine channel is far less than simple channels regarding the unsteady two-phase pressure drop for both channels. As shown in Fig. 21b, in initial times the pressure drop of both channels increased due to temporary blockage of channel by the injected droplets. During the time and movement of droplets, they accumulate in elbows. In the simple channel, the airflow does not pass through the corner of elbows and this leads to accumulation of water in the elbows and forming the slugs until the air momentum and viscous forces dominate the wall adhesion force. Then, this slug starts to move and blocks the major parts of channel leading to instantaneous increase of pressure drop as shown in Fig. 21b. But, in the filleted channels the slugs do not form in the elbows. In addition, the slugs formed in the elbows of simple serpentine channel are large leading to pressure drop. In the simple channels, usually there are some droplets in the elbows leading to pressure drop in end of simulation time.

### 3.3 Experimental validation

In order to validate numerical results with experiments, an experimental setup for simple straight and serpentine channels is designed as shown in Fig. 22. Water is injected to channel by means of a micro syringe pump exactly with same amount of numerical simulation. The data acquisition system is designed using LabView 15 to integrate the micro syringe pump (UMP3-2 with SYS-Micro4 Controller, World Precision Instruments), air flow meter (F-101D, Bronkhorst) and high-speed camera (Phantom MIRO-4, Vision Research). The channels walls (hydrophilic surface) and gas diffusion layer (hydrophobic surface) are made from

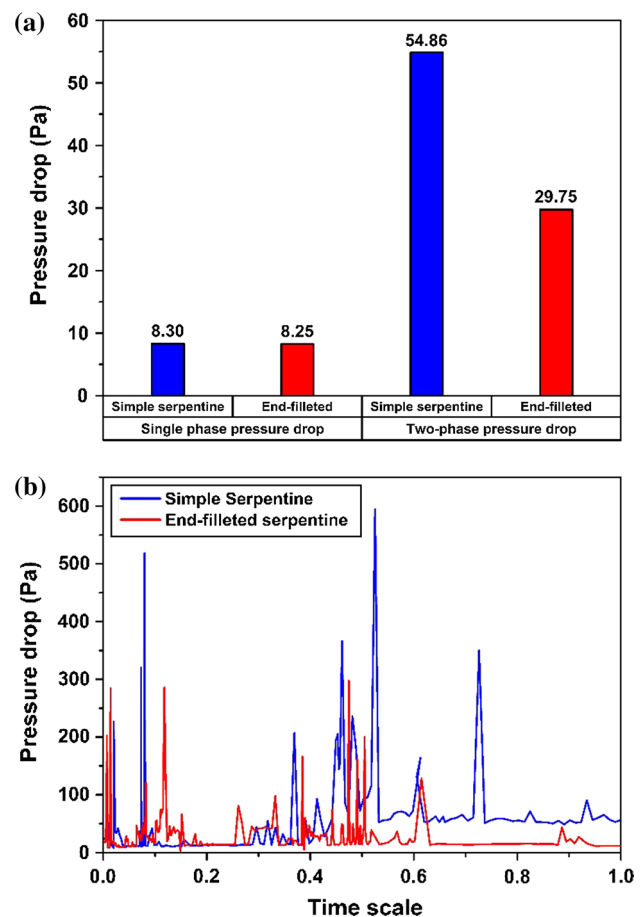


**Fig. 21** Comparison of pressure drop of simple and filleted serpentine channel **a** single and two-phase pressure drop **b** unsteady two-phase pressure drop

Plexiglas and teflonated carbon papers (TGP-H-090, Toray), respectively. The flow parameters and properties of materials and surfaces in simulations and experiments are identical.

In the simple straight channels, departure times of droplets with radii of 31.25 (h/8), 50 (h/5) and 125 (h/2)  $\mu\text{m}$ , are selected as validation parameters, which their distances from channel outlet are 0.9 mm as shown in Fig. 23a. The channel length is 4 mm in order to ensure that the flow profile in the initial droplet location is fully developed and parabolic. In Fig. 23b, the droplet completely left the channel. Departure times of droplet are calculated and compared with experimental data for velocities of 5, 10 and 15 m/s. The experiments are repeated 10 times, and the average of experimental departure times of droplet are calculated while the data repeatability is 96.29 %. As shown in Fig. 24, the numerical results are consistent with experimental data, and the average error is 6.85 %.

In serpentine channels, water coverage ratio of elbows is calculated for experimental validation of numerical simulations. Water coverage ratio is the ratio of the area of

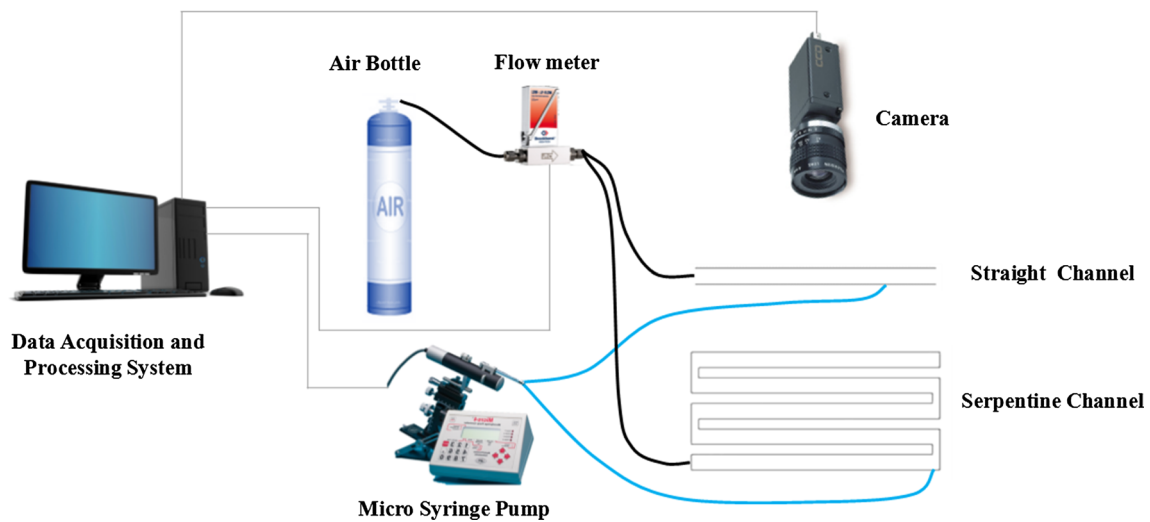
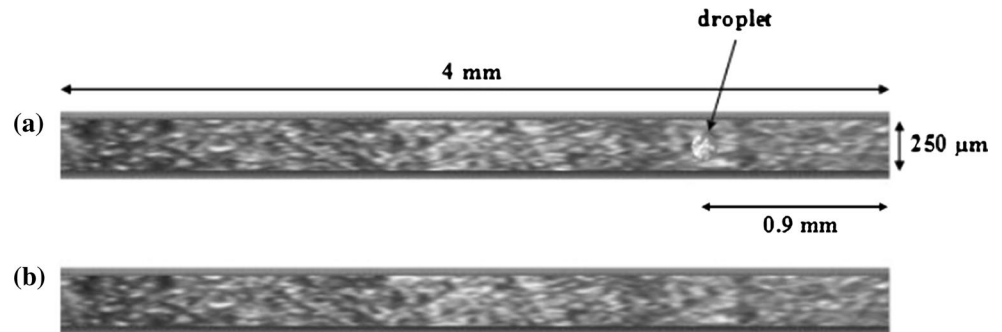


Fig. 22 Schematic of experimental setup for validation

Fig. 23 Droplet in simple straight channel



elbows covered by water to the total area of elbows. Water coverage ratio of elbows is calculated by image processing methods in ImageJ 1.47 software. Before start of the experiments, a video of channel with no droplet (dry video) is recorded, and reference image (dry image) is processed by averaging frames of dry video eliminating any likely noise, and then the reference image is converted to a grayscale image. After this procedure, the air enters the channel, and the droplet is injected to the channel by means of the micro syringe pump, and video recording is started. The frames of the experiment video are converted to a series of grayscale images as shown in Fig. 25a. The difference image is processed by differencing the dry and experiment images. The water is detected using threshold values referring to the water pixels of the difference image, so the threshold image is processed. Due to the similarity of pixels values in the difference image, some other irrelevant pixels are detected as water, so the morphological image processing operations are used to improve the accuracy of water detection

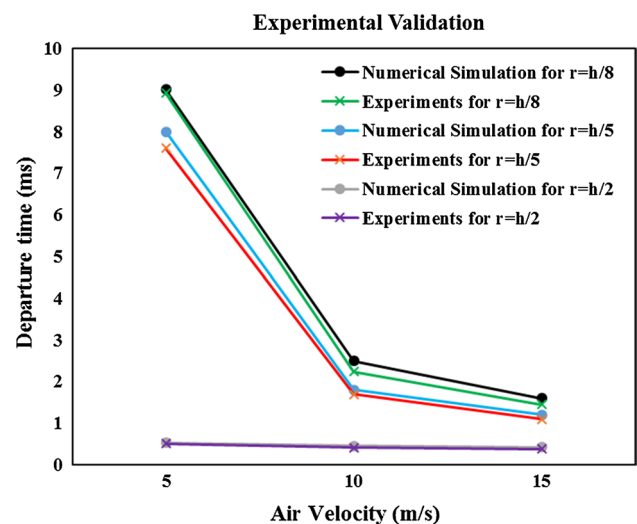
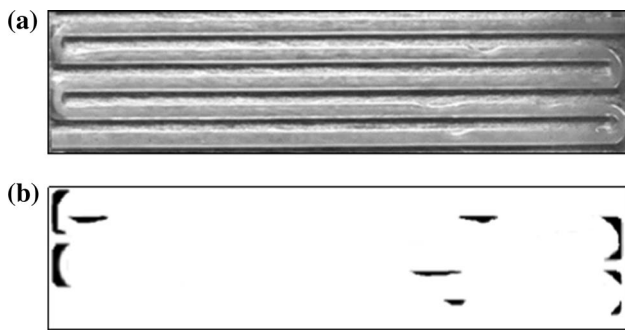
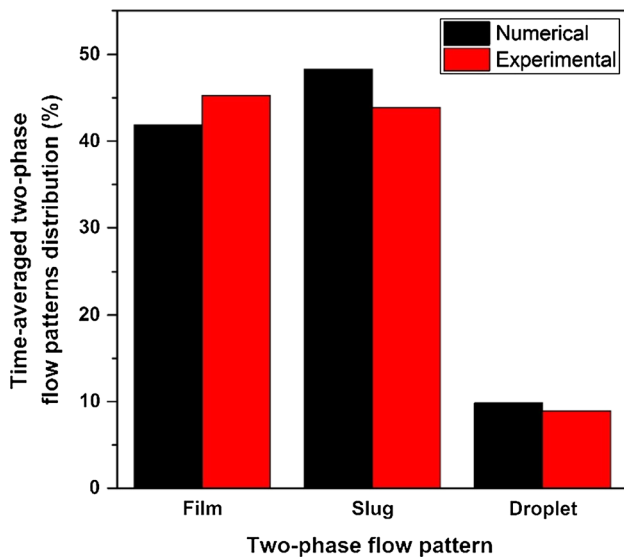


Fig. 24 Departure times of numerical simulation and experiments (simple straight channels)



**Fig. 25** Water coverage ratio (**a** experiment image, **b** final processed image)



**Fig. 26** Time-averaged flow pattern distribution

in the channel achieving more precise results. Finally, the final processed image (binary image) is processed in which the detected pixels as water are shown by black pixels, and other areas are shown by white pixels, as shown in Fig. 25b. The elbows regions are extracted from the other regions by masking the final processed image. The experimental water coverage ratio of elbows (Fig. 25b) is 67 % which its difference with numerical simulation is just 3 % and the relative error is 4.4 %. As stated by Hussaini and Wang [8], the two-phase flow patterns in microchannels of PEM fuel cells are in the forms of droplet, film and slug flow. The time-averaged two-phase flow patterns distribution in the numerical simulation and experiments are given in Fig. 26, and the time steps for image processing is 0.1 (s). The relative error is <7 %, so the numerical simulation data of two-phase flow patterns distribution is in a satisfactory agreement with experimental data. The dominant two-phase flow patterns are slug and film flows, while the distribution of droplet flow is relatively low.

## 4 Conclusions

In the current study, we found the optimal flow-fields between simple and tapered straight channels by utilizing movement mechanism of droplets with different diameters in different operating conditions and detecting the dominant force exerted on droplets. Various parameters of both channels are investigated including water adhered to hydrophilic surface, unsteady and time-averaged two-phase pressure drop and departure time of droplet. In the next part, simple serpentine channels with sharp elbows are optimized from the perspective of water management and lowering pressure drop introducing an optimized filleted channel. The particular conclusions drawn from this study could be listed as follows:

- The momentum was the dominant force for the large droplets ( $r = 125 \mu\text{m}$ ), so their movement mechanisms were translational. For the small droplets ( $r = 50$  and  $31.25 \mu\text{m}$ ), the momentum force was reduced compared to surface tension force so that it could not change the form of droplet, so they had rolling movement. Due to the change in the mechanism of droplet motion from the translational to the rolling mechanism, departure time for the smaller droplets was much further than the largest.
- The pressure drop and pressure fluctuation of tapered channel were getting lower than the simple channel by dispersing of the droplet over the departure time because of further film flow formation on the upper surface compared to the simple channel, which was desirable for the water removal of PEMFCs.
- For the small droplets ( $r = 50$  and  $31.25 \mu\text{m}$ ), the fluctuation of pressure drop over the departure time was lower.
- The amount of adhered water to hydrophilic surface increased by increasing the airflow velocity. It increased by tapering of channel because the height of channel decreased in the tapered channels. No water adheres to the upper surface at the velocity of 5 m/s for simple channel unlike the tapered channel.
- The water coverage ratio of elbows for filleted and simple serpentine channel were 70 and 12 %, respectively. Therefore, the area of oxygen passage was significantly increased in the filleted channel.
- It was shown that the two-phase pressure drop of filleted serpentine channel was far less than simple channels regarding the unsteady two-phase pressure drop for both channels.
- In the filleted serpentine channels, the slugs did not form in the elbows, while the slugs formed in the elbows of simple serpentine channel were large leading to pressure drop.

- The dominant two-phase flow patterns for simple serpentine channel were slug and film flows, while the distribution of droplet flow was relatively low.

## References

- Mehta V, Cooper JS (2003) Review and analysis of PEM fuel cell design and manufacturing. *J Power Sources* 114(1):32–53. doi:10.1016/S0378-7753(02)00542-6
- Kanani H, Shams M, Hasheminasab M, Bozorgnezhad A (2015) Model development and optimization of operating conditions to maximize PEMFC performance by response surface methodology. *Energy Convers Manag* 93:9–22. doi:10.1016/j.enconman.2014.12.093
- Bozorgnezhad A, Shams M, Ahmadi G, Kanani H, Hasheminasab M (2015) The experimental study of water accumulation in PEMFC cathode channel. In: ASME/JSME/KSME 2015 joint fluids engineering conference. American Society of Mechanical Engineers, pp V001T022A004–V001T022A004. doi:10.1115/AJKFluids2015-22299
- Hasheminasab M, Bozorgnezhad A, Shams M, Ahmadi G, Kanani H (2014) Simultaneous investigation of PEMFC performance and water content at different flow rates and relative humidities. In: ASME 2014 12th international conference on nanochannels, microchannels, and minichannels collocated with the ASME 2014 4th Joint US-European Fluids Engineering Division Summer Meeting. American Society of Mechanical Engineers, pp V001T007A002–V001T007A002. doi:10.1115/ICNMM2014-21586
- Srinivasan S (2006) Fuel cells: fundamentals to applications. Springer, New York. doi:10.1007/0-387-35402-6
- Owejan JP, Gagliardo JJ, Sergi JM, Kandlikar SG, Trabold TA (2009) Water management studies in PEM fuel cells, part I: fuel cell design and in situ water distributions. *Int J Hydrogen Energy* 34(8):3436–3444. doi:10.1016/j.ijhydene.2008.12.100
- Yamauchi M, Sugiura K, Yamauchi T, Taniguchi T, Itoh Y (2009) Proposal for an optimum water management method using two-pole simultaneous measurement. *J Power Sources* 193(1):1–8. doi:10.1016/j.jpowsour.2009.02.078
- Hussaini IS, Wang C-Y (2009) Visualization and quantification of cathode channel flooding in PEM fuel cells. *J Power Sources* 187(2):444–451. doi:10.1016/j.jpowsour.2008.11.030
- Ous T, Arcoumanis C (2007) Visualisation of water droplets during the operation of PEM fuel cells. *J Power Sources* 173(1):137–148. doi:10.1016/j.jpowsour.2007.04.075
- Akhtar N, Qureshi A, Scholta J, Hartnig C, Messerschmidt M, Lehnert W (2009) Investigation of water droplet kinetics and optimization of channel geometry for PEM fuel cell cathodes. *Int J Hydrogen Energy* 34(7):3104–3111. doi:10.1016/j.ijhydene.2009.01.022
- Ding Y, Anderson R, Zhang L, Bi X, Wilkinson DP (2013) Simulations of two-phase flow distribution in communicating parallel channels for a PEM fuel cell. *Int J Multiphase Flow* 52:35–45. doi:10.1016/j.ijmultiphaseflow.2012.12.001
- Zhu X, Sui PC, Djilali N (2007) Dynamic behaviour of liquid water emerging from a GDL pore into a PEMFC gas flow channel. *J Power Sources* 172(1):287–295. doi:10.1016/j.jpowsour.2007.07.024
- Zhu X, Sui PC, Djilali N (2008) Three-dimensional numerical simulations of water droplet dynamics in a PEMFC gas channel. *J Power Sources* 181(1):101–115. doi:10.1016/j.jpowsour.2008.03.005
- Jiao K, Zhou B, Quan P (2006) Liquid water transport in straight micro-parallel-channels with manifolds for PEM fuel cell cathode. *J Power Sources* 157(1):226–243. doi:10.1016/j.jpowsour.2005.06.041
- Le AD, Zhou B (2008) A general model of proton exchange membrane fuel cell. *J Power Sources* 182(1):197–222. doi:10.1016/j.jpowsour.2008.03.047
- Le AD, Zhou B (2009) A generalized numerical model for liquid water in a proton exchange membrane fuel cell with interdigitated design. *J Power Sources* 193(2):665–683. doi:10.1016/j.jpowsour.2009.04.011
- Ding Y, Bi HT, Wilkinson DP (2010) Three-dimensional numerical simulation of water droplet emerging from a gas diffusion layer surface in micro-channels. *J Power Sources* 195(21):7278–7288. doi:10.1016/j.jpowsour.2010.05.059
- Theodorakakos A, Ous T, Gavaises M, Nouri JM, Nikolopoulos N, Yanagihara H (2006) Dynamics of water droplets detached from porous surfaces of relevance to PEM fuel cells. *J Colloid Interface Sci* 300(2):673–687. doi:10.1016/j.jcis.2006.04.021
- Kumbur EC, Sharp KV, Mench MM (2006) Liquid droplet behavior and instability in a polymer electrolyte fuel cell flow channel. *J Power Sources* 161(1):333–345. doi:10.1016/j.jpowsour.2006.04.093
- Cho SC, Wang Y, Chen KS (2012) Droplet dynamics in a polymer electrolyte fuel cell gas flow channel: forces, deformation, and detachment. I: theoretical and numerical analyses. *J Power Sources* 206:119–128. doi:10.1016/j.jpowsour.2012.01.057
- Bozorgnezhad A, Shams M, Kanani H, Hasheminasab M, Ahmadi G (2015) The experimental study of water management in the cathode channel of single-serpentine transparent proton exchange membrane fuel cell by direct visualization. *Int J Hydrogen Energy* 40(6):2808–2832. doi:10.1016/j.ijhydene.2014.12.083
- Lu Z, White A, Pelaez J, Hardbarger M, Domigan W, Sergi J, Kandlikar S (2008) Investigation of water transport in an ex situ experimental facility modelled on an actual DOE automotive target compliant fuel cell. In: ASME 2008 6th international conference on nanochannels, microchannels, and minichannels. American Society of Mechanical Engineers, pp 1295–1303
- Concus P, Finn R (1969) On the behavior of a capillary surface in a wedge. *Proc Natl Acad Sci* 63(2):292–299
- Litster S, Sinton D, Djilali N (2006) Ex situ visualization of liquid water transport in PEM fuel cell gas diffusion layers. *J Power Sources* 154(1):95–105. doi:10.1016/j.jpowsour.2005.03.199
- Martin J, Oshkai P, Djilali N (2005) Flow structures in a U-shaped fuel cell flow channel: quantitative visualization using particle image velocimetry. *J Fuel Cell Sci Technol* 2(1):70–80
- Brackbill JU, Kothe DB, Zemach C (1992) A continuum method for modeling surface tension. *J Comput Phys* 100(2):335–354. doi:10.1016/0021-9991(92)90240-Y
- Youngs DL (1982) Time-dependent multi-material flow with large fluid distortion. *Numer Methods Fluids Dyn* 24:273–285
- Fluent A 6.3 (2006) Fluent 6.3 User's Guide, Fluent Inc, Lebanon, NH
- Slater JW (2008) <http://www.grc.nasa.gov/WWW/wind/valid/tutorial/spatconv.html>. NASA (NPARC Verification and Validation Web Site)
- Shateri Amiri M (2011) Numerical investigation of tapered channel of PEM fuel cell. Babol Noshirvani University of Technology. <http://mec.nit.ac.ir/ms/ranjbar/home.aspx>
- Bozorgnezhad A, Shams M, Kanani H, Hasheminasab M (2014) Experimental investigation on dispersion of water droplets in the single-serpentine channel of a PEM Fuel cell. *J Dispers Sci Technol* 36(8):1190–1197. doi:10.1080/01932691.2014.974810